Rapid Prototyping J

Interlayer Temperature Optimisation: An Approach to Maximising Strength in the Large-Scale Additive Manufacture of Fibre-Reinforced PETG

Journal:	*Rapid Prototyping Journal*
Manuscript ID	RPJ-04-2024-0164.R1
Manuscript Type:	Original Article
Keywords:	Composite materials, Fused deposition modelling, Polymers, Anisotropy, Adhesion

INTERLAYER TEMPERATURE OPTIMISATION: AN APPROACH TO MAXIMISING STRENGTH IN THE LARGE-SCALE ADDITIVE MANUFACTURE OF FIBRE-REINFORCED PETG

ABSTRACT

Design/methodology/approach: This study investigates the effect of the temperature at the interface between layers on the ultimate tensile strength (UTS) of 3D printed parts made with post-industrial PETG (PIPG).

Purpose: Fibre-reinforced polymers are gaining popularity in large-scale material extrusion, which involves the layer-by-layer deposition of melted polymeric granulates. However, the mechanical performance of 3D printed components is highly influenced by the quality of the interfacial bond between layers. Material data sheets often do not report the extent of this anisotropy, making it challenging to account for during the design stage without mechanical characterisation.

Findings: The study identifies an optimal previous layer temperature (T_p) of 130±10°C, where interlayer bonding and material properties are maximized. An upper limit of 150°C is identified to avoid material sagging and a critical lower bound of approximately 113°C for achieving at least 80% of the maximum part strength. Moreover, the study underscores the importance of considering the effective cross-sectional area due to the ridged surface of printed samples. Recommendations include the use of infrared heat lamps for temperature control to ensure sustained interlayer bonding.

Research limitations/implications: The research does not address long-term effects and environmental factors affecting material properties, suggesting these as areas for future research.

Originality/value: This study's findings are instrumental in establishing optimal printing parameters for large-scale material extrusion, improving the reliability of 3D printed parts in industries like manufacturing and civil engineering.

KEYWORDS

fiber-reinforced polymers; granulate-based material extrusion; anisotropy; interlayer strength; additive construction

NOMENCLATURE

Additive Construction: Additive manufacturing, or 3D printing, applied in the context of the construction industry.

Material Extrusion: A family of 3D printing technologies where a part is produced via the melting and extruding of a feedstock material through a nozzle which follows a predefined list of coordinates to build up the final shape in a layer-by-layer fashion.

Fused Granulate Fabrication: A 3D printing technology in the family of Material Extrusion that uses polymer granulates as the feedstock.

Melt Temperature: The temperature of the polymer as it is extruded and deposited to form a bead.

Previous Layer Temperature: The temperature measured at the top layer of the part, or the temperature of the most recently deposited layer.

Critical Temperature: The lowest acceptable Previous Layer Temperature before poor interlayer adhesion will be anticipated.

INTRODUCTION

Fibre-reinforced polymers are increasingly being employed in the large-scale 3D printing of components across a spectrum of industries, including automotive, aerospace, and construction [1,2]. The 3D printing technique typically utilizes polymeric granulates, with an average particle size ranging from 3-5mm in diameter, as the feedstock for a layer-by-layer material extrusion process closely related to Fused Filament Fabrication (FFF). Due to the use of granulates rather than a filament, this

3D printing process is increasingly referred to as Fused Granulate Fabrication (FGF), although it is referenced in literature by synonymous terms including pellet-based Fused Filament Fabrication, Fused Pellet Fabrication, or Fused Granular Fabrication [3,4,5]. The materials used in FGF closely resemble those used in injection moulding, and as a result, technical data sheets often provide information more pertinent to injection moulding, where material properties are typically assumed to be isotropic. This approach is inadequate for 3D printing due to the layered nature of the printing process, where mechanical performance is largely attributed to the quality of the bond between layers. Previous studies have demonstrated this phenomenon, showing that 3D printed polymeric composites have lower measured strength when loaded out-of-plane with respect to the layer axis [6,7].

Further, even when materials are tested specifically for FGF applications, the testing often takes place under ideal climatic conditions with consistent layer times to ensure an optimal bond between layers and maximum out-of-plane strength. While this is an aspirational standard, it is typically impractical for large-scale 3D printing projects. More complex geometries necessitate inconsistent layer times, and the scale of printer means climatic factors are significantly more expensive to control, for example through a temperature-controlled print chamber.

The studies presented herein were performed in advance of a large-scale 3D printing project where the above concerns were prominent, and is discussed in detail in Storey et al. [8](forthcoming). The project aimed to employ a recycled and short fibre-reinforced grade of polymer. Given the multifaceted interactions between physical properties and manufacturing constraints, representative part testing was deemed a practical means of assessing the functional strength of the components to be manufactured. Consequently, the horizontal (X) and vertical (Z) orientations were evaluated as illustrated in Figure 1 below. The goal was to capture the variation in mechanical performance in the two directions, and interpolate for orientations in between, with the aim of using this information to inform the design and the manufacturing setup necessary to achieve the desired mechanical strength.

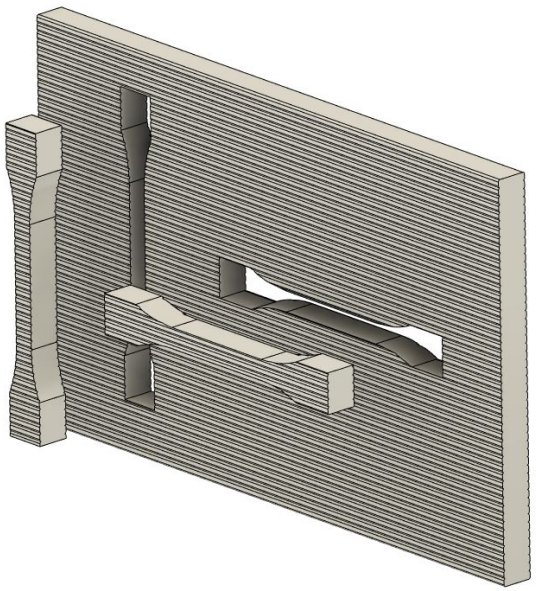

Figure 1: Illustration of directions discussed in this paper. Left: Vertical (Z-direction). Right: Horizontal (X-direction). Figure by authors.

This study posits that the temperature at the interface between layers during material deposition is critical for ensuring strong interlayer adhesion. Melt temperature, $T_{m,}$ is the temperature above which a material flows readily as a liquid and offers the best conditions for interlayer molecular diffusion, but maintaining interlayer temperatures above T_m is not practicable, as even if a heated chamber could sustain that temperature, the printed part would fail to retain the intended shape. However, many polymeric materials can still act as semi-viscous solids much below this T_m, depending on the crystalline structure [9]. This

property of polymers is leveraged for 3D printing, ensuring the intended shape is maintained while still allowing interlayer bonding to occur. A commonly referenced parameter is the glass transition temperature, T_g, which refers to the temperature at which polymers transition from fully solid toward a "rubbery" state. The temperature region between T_g and T_m is known as the glass transition region. This temperature region is typically identified by changes in the material's mechanical and thermal properties, such as its modulus of elasticity, specific heat capacity, and thermal expansion coefficient, and could be a good indicator of when interlayer bonding will cease to occur. A hypothesis was proposed that to ensure a good bond, the temperature at the contact surface between the previous and new layers should be higher than T_g. This contact temperature is difficult to precisely measure with certainty; the only knowns are the temperature of the polymer exiting the extruder (which is close to T_m) and the temperature of the previous layer immediately prior to the next layer being deposited, T_p. These values are illustrated in Figure 2.

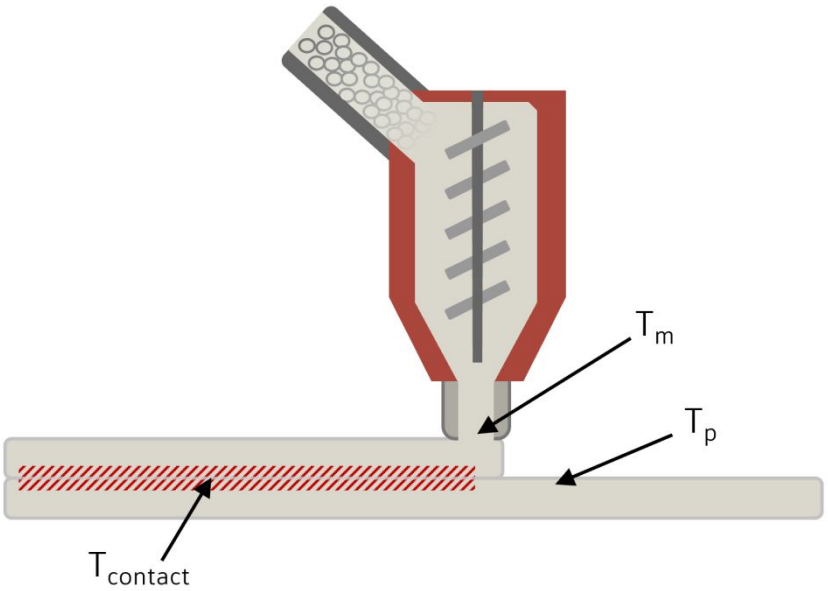

Figure 2: An illustration of a theoretical temperature between 3D printed layers. An initial assumption was that this must be greater than the glass transition temperature to ensure a good bond. Figure by authors.

The literature on the glass transition region shows some variability in consensus. Kalogeras and Hagg Lobland [9] highlight this ambiguity, stating:

> *"Different operational definitions of the glass transition temperature T_g are in use, and several of them are endorsed as accepted scientific standards. Nevertheless, all definitions are arbitrary, and all yield different numeric results."*

Additionally, polymers that are recycled and contain chopped fibre reinforcement are unlikely to exhibit the same T_g as virgin material. The mechanical and thermal cycles in the recycling process can introduce variability in the length and distribution of polymer chains. This results in fluctuations in the weight-average molecular weight, M_w, which in turn leads to recycled polymers exhibiting a broader range of T_g values instead of a singular, consistent value [10,11,12]. Additionally, fibre reinforcement will likely restrict motion of polymer chains, making it harder for them to move past each other and thereby impact the transition into the rubbery state. Thus, it is not appropriate to conclude a minimum temperature for interlayer bonding without further experimentation. Nevertheless, literature on the glass transition temperature suggests the T_g of virgin PETG is 75-88°C [12,14,15,16], so this information was therefore the first assumption when defining studies for this paper.

It was further hypothesised that the strength of the material perpendicular to its layer direction, hereafter abbreviated to "Z-strength", would follow a curve as shown in Figure 3. Material strength would increase as temperature increases because more thermal energy will allow for better molecular diffusion and improved material adhesion between layers. At the higher end of the temperature range, it was suggested that there will be a sudden end to the curve after some critical point, with the material slumping (deforming or sagging due to heat) to the extent that testable specimens can no longer be extracted. On the

lower end of the temperature range, the material will reach a point where negligible bonding occurs and any small force will separate the layers. Beyond these upper and lower limits, it will not be possible to manufacture a representative specimen for testing.

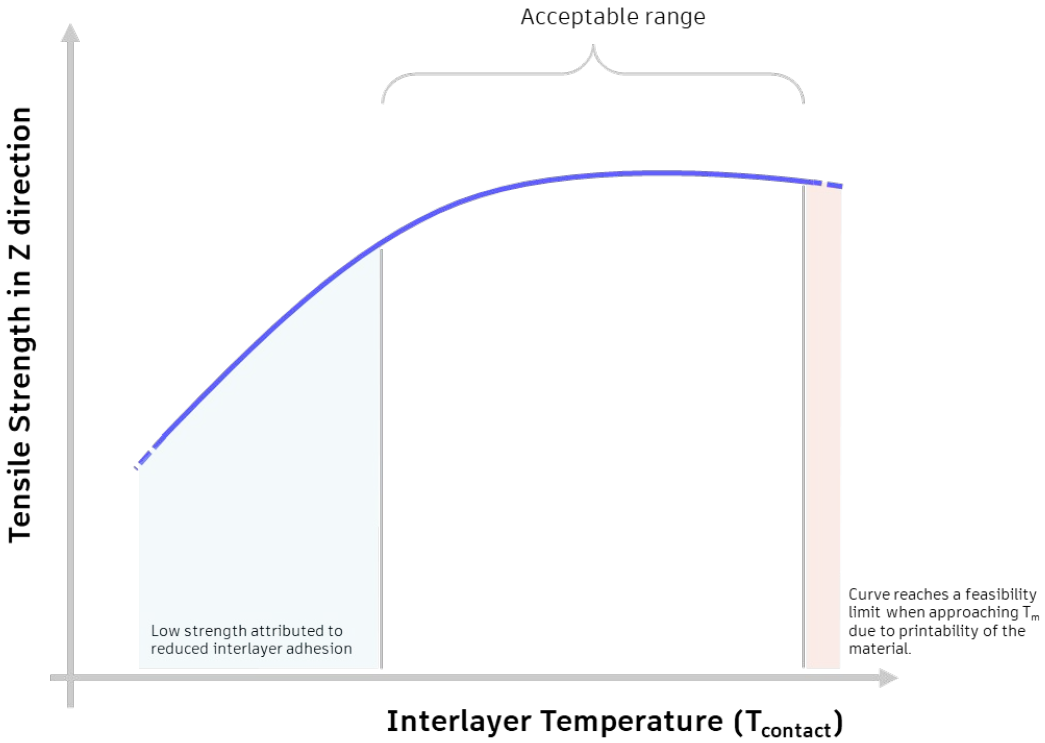

Figure 3: Hypothesised relationship between tensile strength and interlayer temperature. Figure by authors.

With this considered, there will be an acceptable range of interlayer temperatures that each layer of the part should be printed within. If the temperature is too high, the polymer will not be solid enough to support its own weight and will begin to collapse. If the temperature is too low, the bond will be too weak to meet performance criteria. The acceptable temperature range will vary depending on the project: parts that require lower mechanical performance may have a wider range of acceptable temperatures. Experimentation is hence required to determine the boundaries of this acceptable range for the given project and material.

In Fused Granulate Fabrication, the time taken to print a single layer can often be long and inconsistent. There is a need for temperature monitoring and correction to ensure the part stays within the acceptable range illustrated above. Previous work from Kishore et al. [11] looked at preheating parts with infrared (IR) heat lamps to re-elevate the material temperature above T_g immediately before the next bead is laid down, but they observed minimal increase in tensile strength compared with no IR reheating at all. A possible oversight in this approach is the brevity with which the heat is applied, which may act to superficially warm the surface of the bead, but not provide enough thermal energy to reheat the core of the bead. It is likely that the thermal mass of the part helps to drive a stronger interlayer bond. Other work by Wang et al. [17] has explored the use of directed lasers to rapidly and locally reheat the previous layer above the material's T_m. This approach eliminates the necessity to maintain a high temperature through the entire layer, and is quoted to significantly increase flexural strength in the Z-direction. The drawbacks of this approach are that it will not reduce part warping when used in isolation of other temperature control measures, and it introduces additional hardware integration and safety considerations.
These methodologies are critical in many projects using FGF, but were not necessary for the purposes of producing the smaller samples for mechanical testing presented in this paper.

This research aims to explore the interplay between interlayer bonding, temperature, and the mechanical performance of fibre-reinforced polymers in FGF. The focus lies on understanding how the temperature between layers during the printing process affects the final product's strength, particularly in the Z-direction. This research also seeks to establish a temperature range that allows for optimal interlayer adhesion without compromising the shape and integrity of the printed part. In doing so, it aims to provide valuable insights that can guide the design and manufacturing setup for future large-scale additively manufactured objects.

MATERIALS & METHODS

Several materials were evaluated as candidates for the project described in Storey et al. [8](forthcoming), using three primary criteria: printability, sustainability, and performance. The candidate materials had resins of either polyethylene terephthalate (PET), polyethylene terephthalate glycol (PETG), or polycarbonate (PC), and were reinforced with either carbon or glass fibres.

Printability: The material should print consistently, quickly, and demonstrate a high level of repeatability. There should be sufficient tolerance in moisture content, melt temperature and residency time in the extruder to allow for thousands of kilograms of material to be printed without risk of maintenance downtime. The visual appearance as assessed by the consistency of the print bead was also deemed highly important because, although based on a relatively subjective and aesthetic assessment, a consistent bead quality infers a reliable extrusion rate and a lower chance of defects as ever greater numbers of layers are added on top of each other during large scale fabrication [10].

Sustainability: Favour was given to recycled grades of material, with the possibility for repeated recycling at the end of the product's lifespan. Therefore, the source of the polymer resin (e.g., post-consumer, post-industrial) and the type of fibre (e.g., glass, carbon) were compared. Given the intent to recycle the material at the end of the product's lifetime, material degradation after multiple melt cycles was discussed but not tested within the scope of this project.

Performance: The material must offer sufficient strength for use in a civil infrastructure project. Technical data sheets provided by suppliers offer enough insight for initial comparison between available options, despite missing key data such as multi-directional tensile and compressive strength.

Sustainability and performance criteria were assessed based on the available data provided by material suppliers, while printability was tested by comparing the quality of standard geometries, as shown in Figure 4. Following this assessment, the material selected was a Post-Industrial PETG (PIPG) with 30% content of 4.5mm-long chopped glass fibre, supplied by Mitsubishi Chemical Performance Polymers (MCPP). The mechanical properties of this material, as indicated in its Technical Data Sheet, suggested a good degree of suitability for this study. In-house trials demonstrated excellent printability and compatibility with the equipment used in this study. The post-industrial resin source demonstrated an active step toward sustainable sourcing.

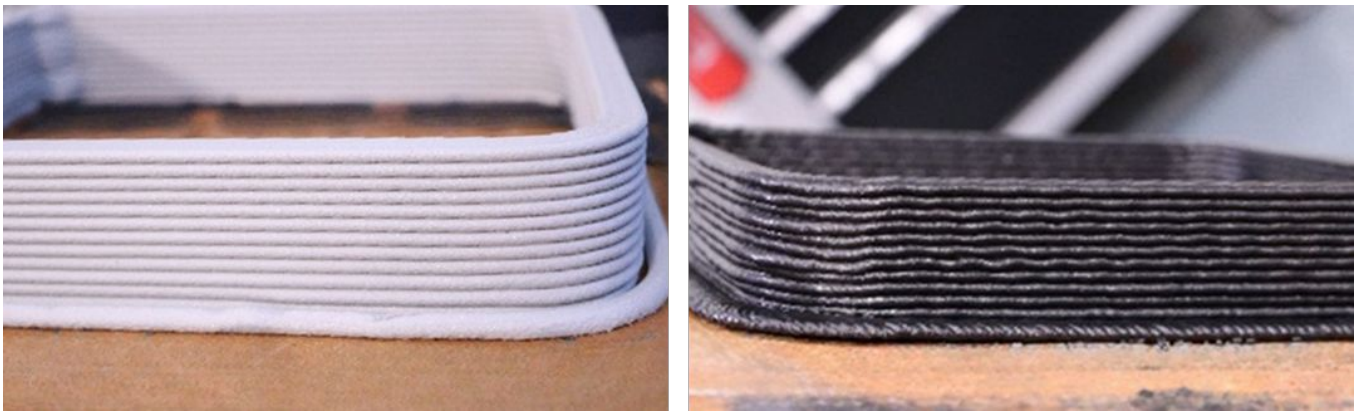

Figure 4: Standard geometries from two of several candidate materials tested. Left: The chosen material of PETG with 30% glass fibre. Right: PET with 35% carbon fibre. The PET material exhibited lower printability, as can be inferred from the visual quality of the bead. Carbon fibre also has a higher embodied carbon than glass fibre, which contributed to the choice of a glass fibre-reinforced polymer. Figure by authors.

Specimen Manufacture and Temperature Measurement

Specimens were produced in two different facilities with different extruder and robot arm architectures at each facility. This study did not aim to compare the performance of different extruders with rigor and findings should not infer a recommendation.

The first set of specimens were produced by printing vertical-walled parts using a CEAD E25, a pellet extruder with four heat bands hereafter referred to as Extruder A. This extruder was mounted to an ABB IRB6700 6-axis robot arm. The test specimens were subsequently cut from the printed parts with an OMAX ProtoMAX waterjet cutter. The second set of specimens was printed using a HMT XTRUDE, a pellet extruder with a single heat band hereafter referred to as Extruder B. This extruder was mounted to a KUKA KR210 6-axis robot arm. Here, the test specimens were cut using a milling spindle attached to another KR210 robot arm.

In both setups, the temperature was monitored at the same x,y coordinates for every layer, using a Micro-Epsilon thermoIMAGER TIM QVGA thermal imaging camera. This temperature was manually recorded immediately prior to the extruder passing with the subsequent layer of material, thereby giving a value for the previous layer temperature T_p in °C. Due to the relatively small size of the samples and the high probability of anomalies in temperature measurement obfuscated by the heat of the extruder, it was decided that manually recording the value of T_p, rather than via an automated system, was most appropriate. The print speed was manually adjusted via the respective robot teach pendant to ensure this temperature remained adequately consistent for every layer of the print.

For all geometries printed, the T_p for any given layer was within ±10°C of the target temperature. The set temperature of all extruder heat bands was kept constant at 230°C, as recommended by the material provider. Both extruders utilised hardened steel nozzles to reduce the impact of abrasion from the fibres and maintain a consistent nozzle diameter for the duration of the build. Due to the hydroscopic nature of PET, the material granulate was dried within a desiccator for at least 4 hours at 65°C to remove absorbed moisture before commencing printing, as recommended by the supplier.

Tensile Specimens

A dog-bone coupon geometry was used based on ISO 527-2 [19] as shown in Figure 5. Due to restrictions in the manufacturing setup, a specimen thickness *h* of 10±1mm was manufactured.

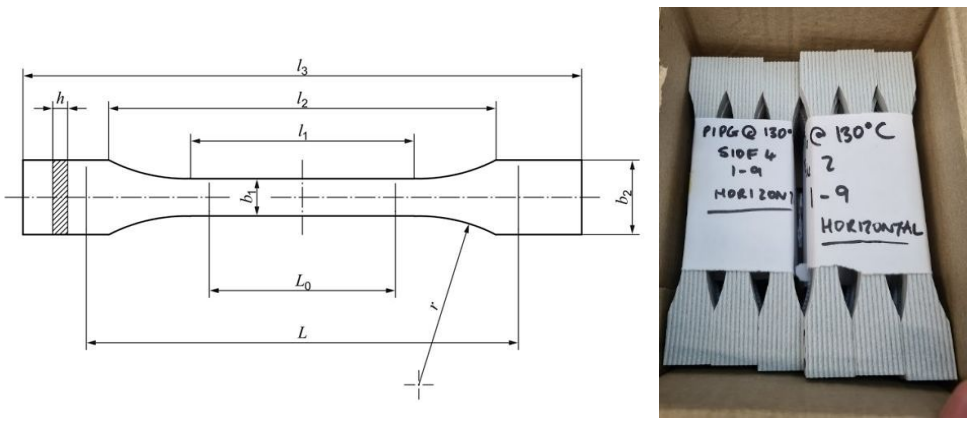

Figure 5: Left: ISO 572-2 1B standard, with dimensions explained in Table 1. Right: A set of Horizontal (X) dog-bone specimens after cutting with a waterjet cutter. Figure by authors.

The dimensions for dog-bone coupon geometry ISO 527-2 1B are displayed in Table 1. To compare the impact of the as-printed surface, some samples were planed using a Tormach CNC machine to remove the ridged surfaces. This is highlighted in the "Preferred thickness" row where the two dimensions, 10±1mm and 6±0.6mm, are the dimensions of the as-printed (AP) and planed (P) samples respectively.

Table 1 Dimensions for dog-bone specimen for ISO 527-2 1B. All dimensions in mm. Table by authors.

l_3	Overall length	≥ 150
l_1	Length of narrow parallel-sided portion	60 ± 0.5
r	Radius	60 ± 0.5
l_2	Distance between broad parallel-sided portions	108 ± 1.6
b_2	Width at ends	2 ± 0.2
b_1	Width at narrow portion	10 ± 0.2
$\boldsymbol{h}$	**Preferred thickness**	4 ± 0.2 ($\mathbf{10 \pm 1}$ ***or*** $\mathbf{6 \pm 0.6}$)
L_0	Gauge length (preferred)	50 ± 0.5
L	Initial distance between grips	115 ± 1

Compressive Specimens

ASTM D695 [20] was used as the basis for compressive strength tests. Walls of two extrusion beads thick, with bead dimensions of 10 x 2mm were printed, allowing cuboidal specimens of 20 x 20 x 40mm to be milled from the printed geometry. To replicate representative loading, the other faces were left with as-printed surface condition. Compressive force was applied to the 20 x 20mm square faces, as illustrated in Figure 6.

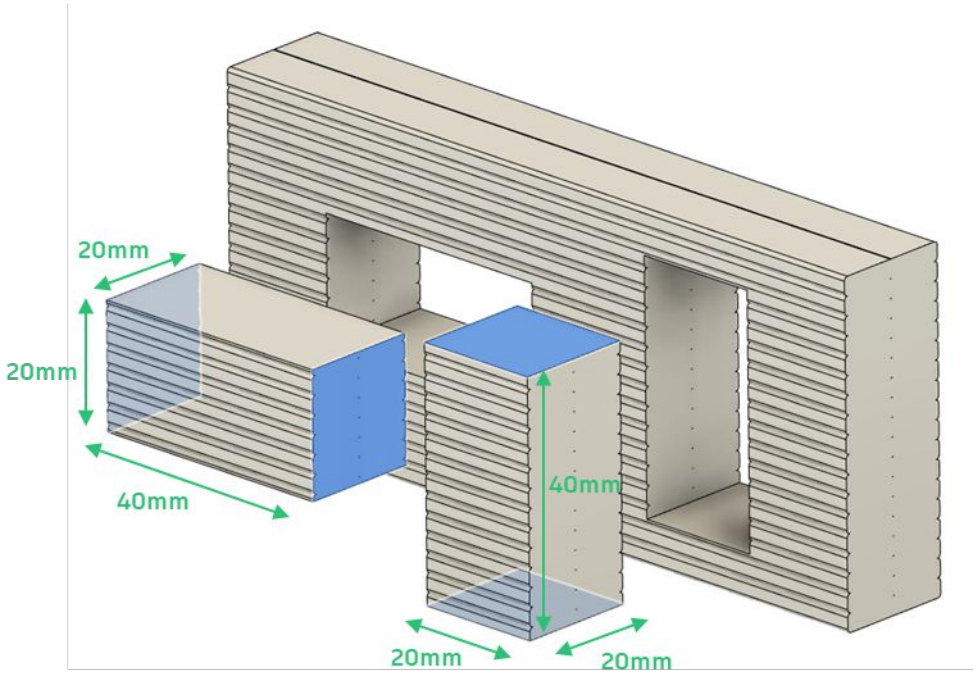

Figure 6: Illustration of specimens created for Compressive Strength tests. Highlighted surfaces represent the faces where loading was applied. Left: Horizontal (X) specimen. Right: Vertical (Z) specimen. Figure by authors.

Shear Specimens

Specimens were produced in accordance with ASTM D5379 V-notched beam testing method [21]. Specimens were cut from prints of the same geometry as tensile specimens: single-walled parts with bead dimensions of 10mm x 2mm. Specimens had dimensions of 76 x 19 x 10mm with a 45° notch with 3.8mm depth. The notches were machined with a 2mm diameter end mill, giving a 1mm radius at the base of the notch. Dimensions are illustrated in Figure 7.

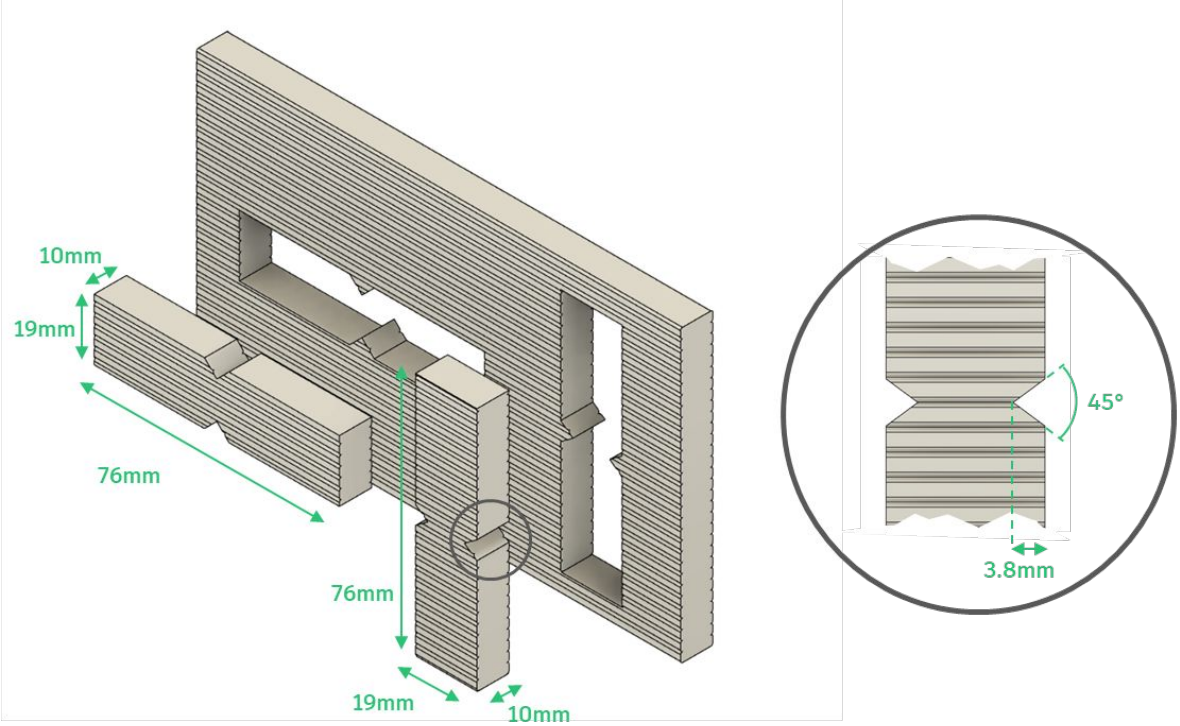

Figure 7: Illustration of specimens created for Shear Strength tests. Left: Horizontal (X) specimen. Middle: Vertical (Z) specimen. Right: Close-up of vertical specimen, with dimensions of the notch. Figure by authors.

Testing Facilities and Equipment

To assess the repeatability and reproducibility of this process, three testing facilities were employed to ratify internal manufacture and testing. For the interlayer temperature study, an external independent company, External A, carried out tests with specimens from Extruder A. Further studies were carried out at a second external independent company, External B, and at an internal facility, Autodesk Materials Lab in Kilsyth, Australia.

At Autodesk Materials Lab, measurement of tensile and compressive properties was performed using the Instron 3367 Universal Testing Machine with a 30kN load cell and an attached video extensometer to measure axial strain. The video extensometer operates via a camera and polarised light source to detect painted dots on the sample to determine the axial strain in the sample during testing. The load cell and video extensometer are regularly calibrated.

For tensile testing, the Instron pneumatic side action grips with a 10kN load rating were used. These grips support a maximum sample thickness of 13mm making it suitable for the specimens. The experiments were carried out as per the ISO527-2 standard with a constant crosshead speed of 5mm/min applied on the sample during the test until the sample

reached failure. Axial strain was measured using the video extensometer and data from the stress-strain curve was used to determine the ultimate tensile strength. The Horizontal (X) specimens were tested at ambient room temperature conditions (22±2°C). The Vertical (Z) specimens were tested at ambient room temperature, and via the use of an environmental chamber set to 70°C and -20°C to simulate environmental conditions.

For compression testing, 100mm diameter Instron compression platens with a 100kN load rating were used. The rectangular block samples were cut from an initial size of 20 x 20 x 40mm to 10 x 10 x 20mm to ensure the force limits of the 30kN load cell were not exceeded. The experiments were performed as per the ASTM D695 standard at a constant crosshead speed of 1mm/min until the compressive force on the sample reached 25kN. The axial strain was measured using the video extensometer and the raw stress-strain data was used to determine compressive modulus, ultimate compressive stress and compressive stress at yield (offset 0.2% strain). The Horizontal (X) specimens and Vertical (Z) specimens were tested at ambient room temperature conditions.

Differential scanning calorimetry (DSC) was performed to determine the glass transition temperature and melt temperature using a TA Instruments Discovery DSC 972000.901. A heating and cooling rate of 20°C/min was used.

RESULTS

Study 1: Differential scanning calorimetry

DSC was conducted to determine the material's T_g and T_m values. Three samples were tested: one from the centre of a compression specimen, and one each from the top and bottom of a tensile specimen. These samples were chosen to verify whether results were acceptably consistent regardless of location in the print, but this dataset is too small to draw conclusions on differences between sample types. Results are displayed in Figure 8.

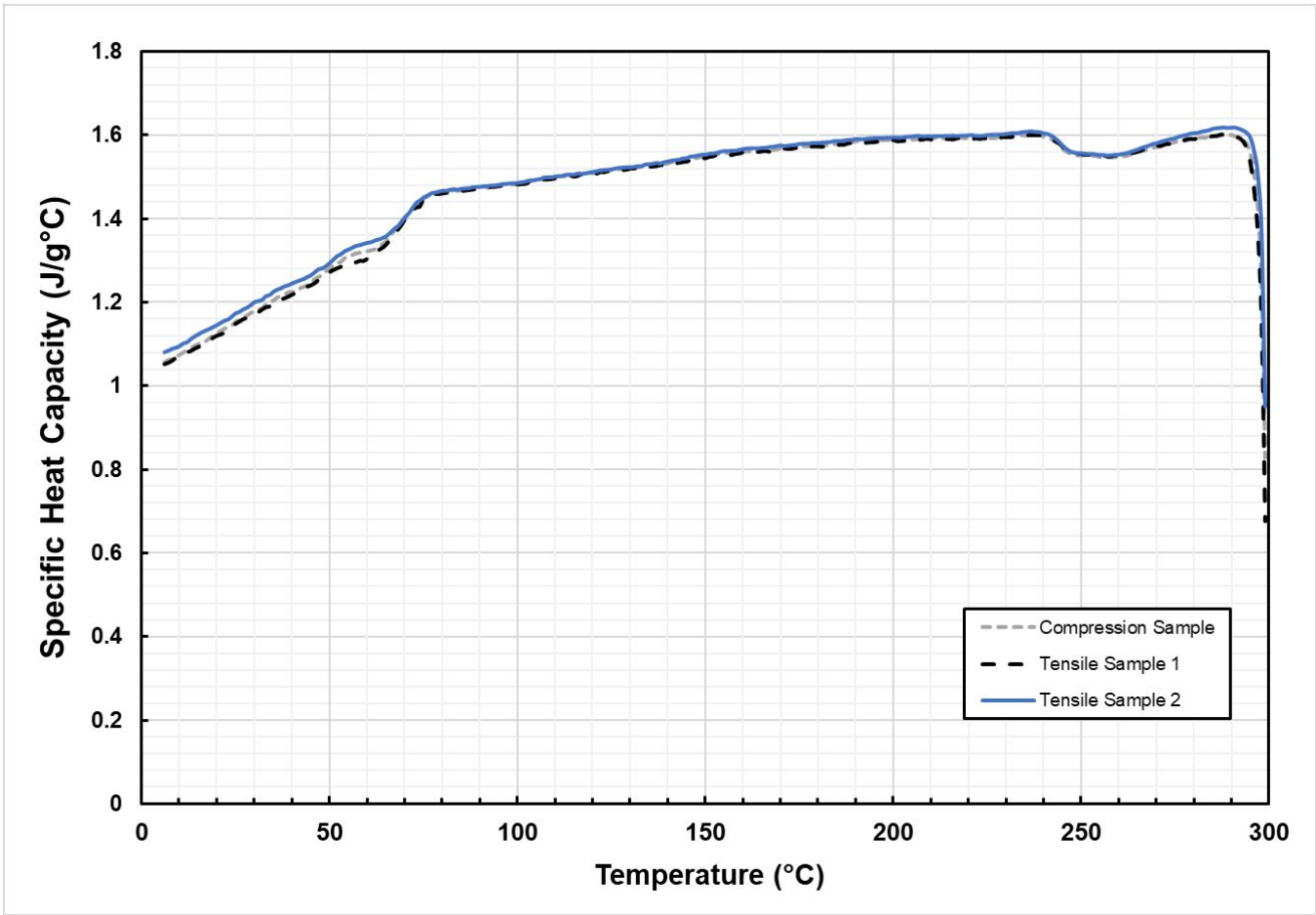

Figure 8: Results from Differential scanning calorimetry (DSC) for 3 samples of Post-Industrial PETG with 30% glass fibre (PIPG), indicating a glass transition range between 60 and 75°C for this material. Figure by authors.

The specific heat capacity results were analysed in accordance with the methods detailed in DSC equipment user manuals [18, 22]. The glass transition was determined to begin at 68.5±1.1°C and end at 74.6±0.3°C. A representative value for Tg was calculated to be 71.8±0.5°C at the midpoint of this transition region. Melting of the material was determined to begin at 242.2±0.4°C and end at 246.9±0.6°C. A representative T_m value of 244.5±0.3°C was calculated at the midpoint of the melting region.

Study 2: The impact of interlayer temperature

To find the optimal temperature as postulated in Figure 3, a set of five vertical (Z-direction) samples were tested for each of five interlayer temperatures, outlined in Table 2 below. The interlayer temperature is not directly measurable or clearly definable. Therefore, this study measured the last known temperature of the previous layer, T_p. A maximum T_p of 150°C was

chosen because it was discovered through initial testing that parts printed above this temperature were too hot to support their own weight. It was hypothesised that the material's T_g would play a role in interlayer molecular diffusion, so a minimum T_p of 70°C was selected given that this is measurably below the T_g observed from in-house DSC during Study 1.
This study used specimens printed with Extruder A and were tested at facility External A. These results are presented in Table 2 and in Figure 9.

Table 2: Ultimate Tensile Stress (UTS) against Previous Layer Temperature, for samples printed with Extruder A and tested by External A. Table by authors.

Previous Layer Temperature, T_p (°C)	Ultimate Tensile Stress (MPa)					Mean UTS (MPa)	Standard Deviation
	Sample 1	Sample 2	Sample 3	Sample 4	Sample 5		
70	20.1	15.2	26.5	28.6	29.6	24.0	6.2
90	24.1	26.1	26.8	28.6	28.9	26.9	2.0
110	28.1	27.8	27.6	23.3	29.4	27.2	2.3
130	32.5	32.2	31.1	31.6	32.2	31.9	0.6
150	28.7	29.0	28.9	28.7	28.8	28.8	0.1

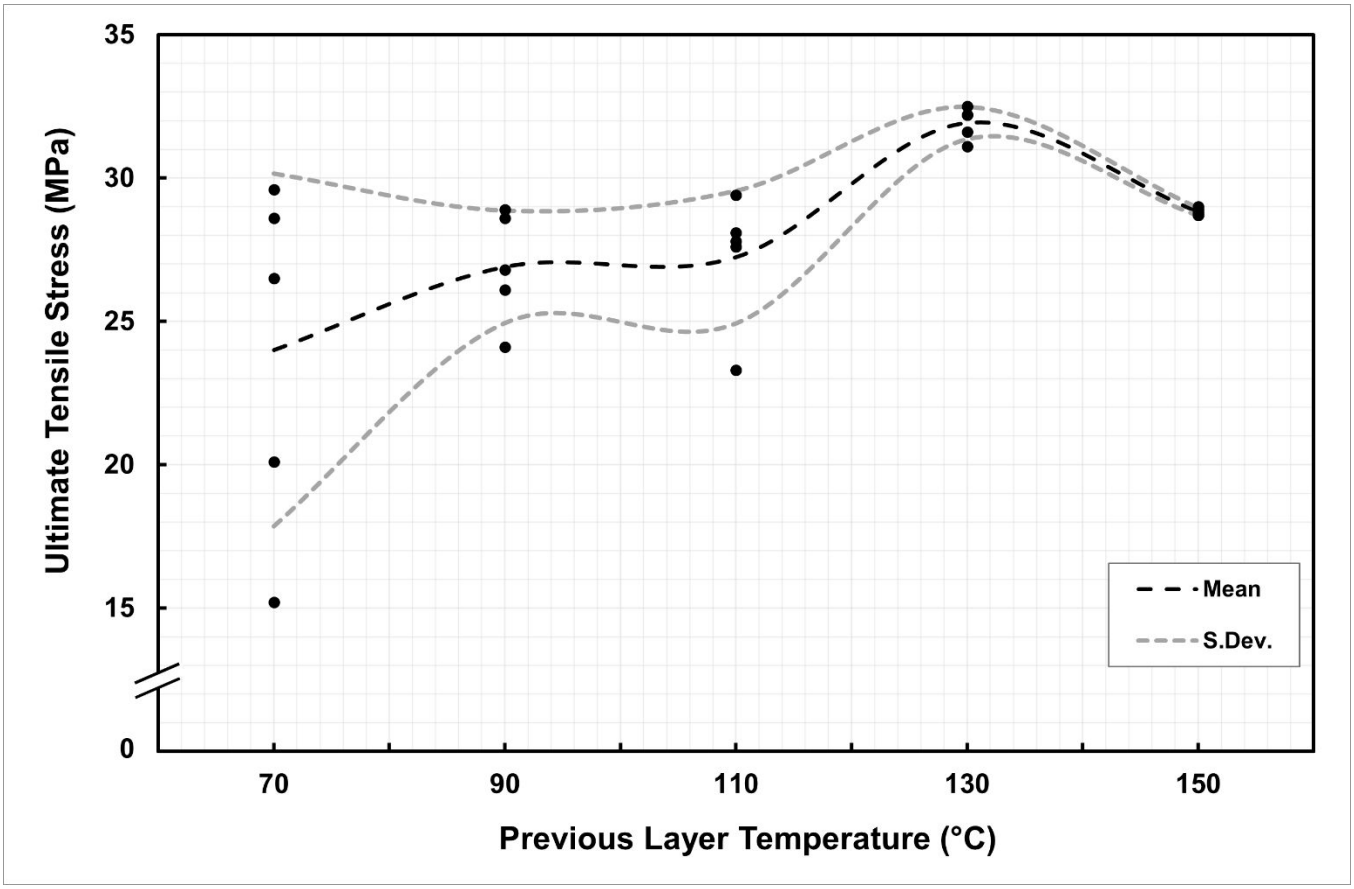

Figure 9: Ultimate Tensile Stress (UTS) against Previous Layer Temperature, for samples printed with Extruder A and tested at facility External A. Smoothed lines are plotted for the mean and standard deviations. These lines do not represent a definitive relationship, but rather act as a guide for the eye between sample groups. The use of dotted lines is a deliberate indicator that these are not definitive trendlines and have a degree of uncertainty. The Y axis was truncated for better visibility of individual data points. Figure by authors.

These results suggest an optimal T_p of 130°C for this manufacturing process and material combination. It was not practical to carry out the subsequent studies in this project with specimens printed with five different T_p values, so all further studies were carried out with specimens printed at the 130°C optimal T_p value identified.

Study 3: Validation of Z-strength at Optimal T_p

To explore the reliability of 130°C as the optimal T_p, specimens from two different extruders were tested. Figure 10 shows stress-strain curves from in-house testing. Figure 11 shows the comparison of data alongside two external testing facilities. Table 3 offers numerical comparison.

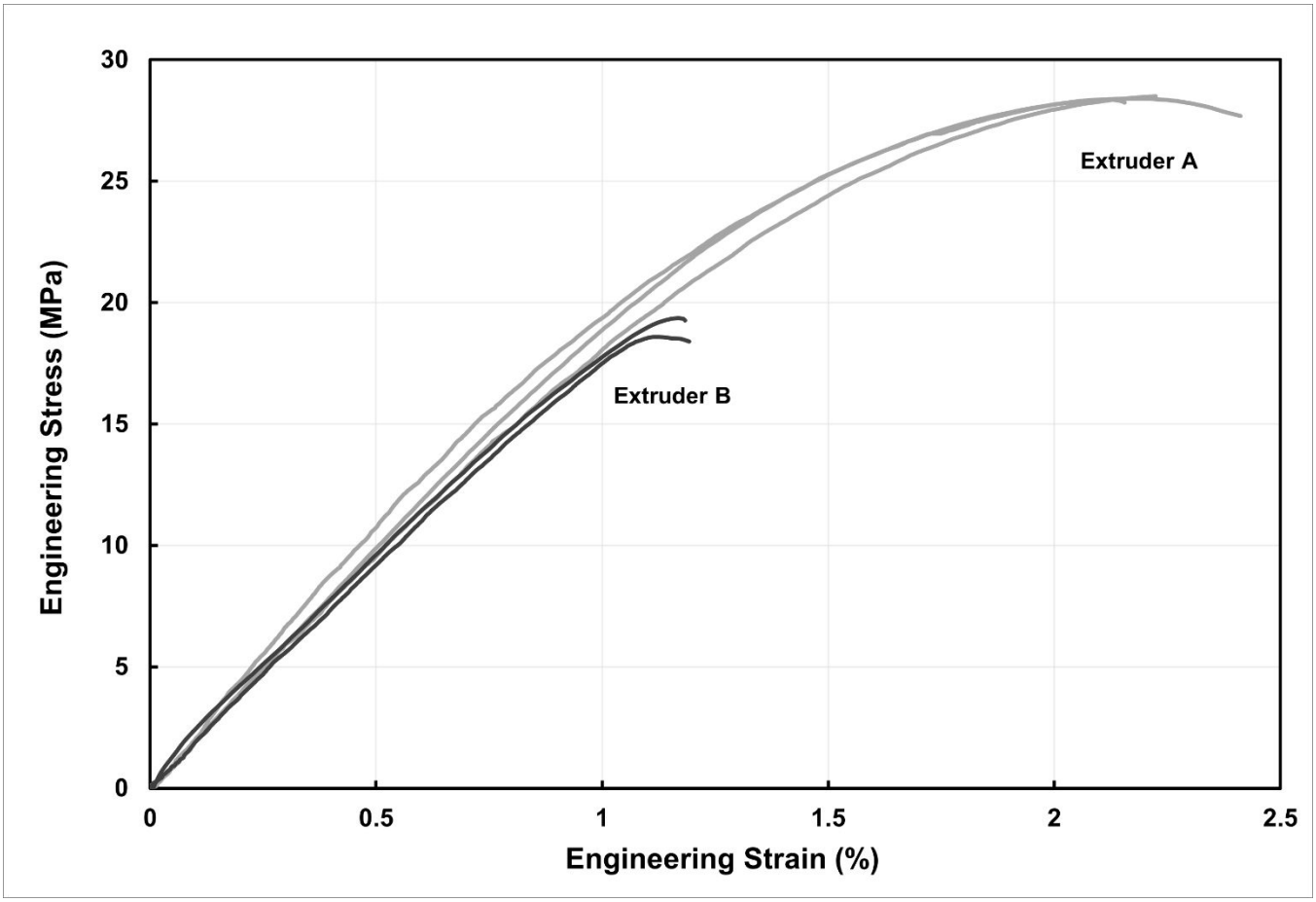

Figure 10: Stress-Strain curves of Z-direction tensile samples, printed with a target T_p value of 130°C, using extruders A and B, and tested internally. Figure by authors.

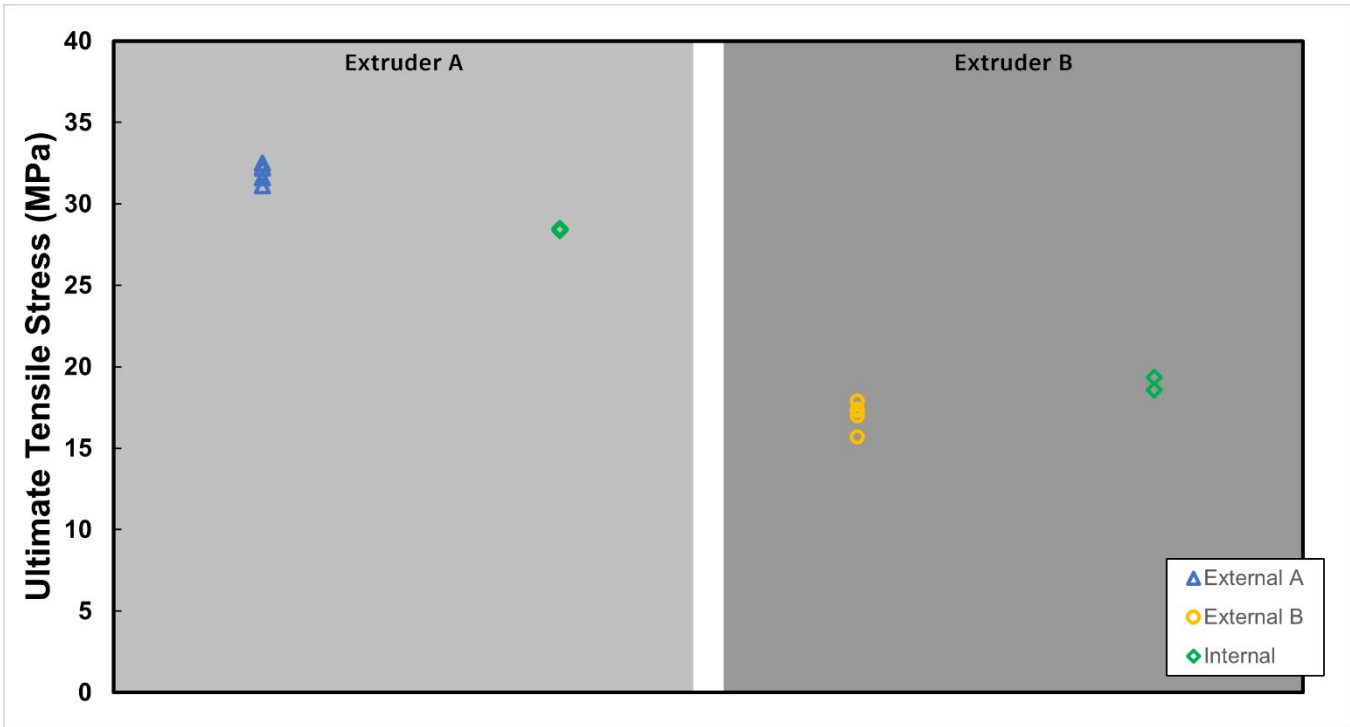

Figure 11: Comparison of the UTS of Z-direction tensile samples, printed with a target T_p value of 130°C, using extruders A and B, tested internally and at two third-party testing facilities. Figure by authors.

Table 3: Tests from specimens printed at 130°C and cut in the Z-direction. Table by authors.

Sample Type	Sample Size	Mean UTS (MPa)	Standard Deviation
Extruder A, tested by External A	5	31.92	0.56
Extruder A, tested by Internal	3	28.42	0.07
Extruder B, tested by External B	4	16.98	0.93
Extruder B, tested by Internal	2	18.97	0.54

The closeness of the mean values, when accounting for small sample sizes, increases the confidence in the results obtained from the three testing facilities. However, there is clear discrepancy between the UTS values recorded for the Extruder A and Extruder B specimens. This study did not attempt to rigorously compare sources of variability between the two manufacturing setups, but despite having identical manufacturing parameters the two manufacturing cells produced samples with measurably different mechanical properties. The key implication for the reader is that printing with the same material, with the same interlayer temperature, and same bead dimensions will not necessarily result in the same interlayer strength as is presented in this paper. Each individual 3D printing setup is likely to present some variation in results. Further work should look to explore this over a larger sample size and with a wider range of extruder architectures.

Study 4: Z-strength vs X-strength

Figure 12 shows the comparison between Z (vertical) and X (horizontal) strength for specimens printed with Extruder A and Extruder B, tested internally. Figure 13 shows UTS values for Z and X directions, including results from third-party testing facilities, with numerical comparison in Table 4.

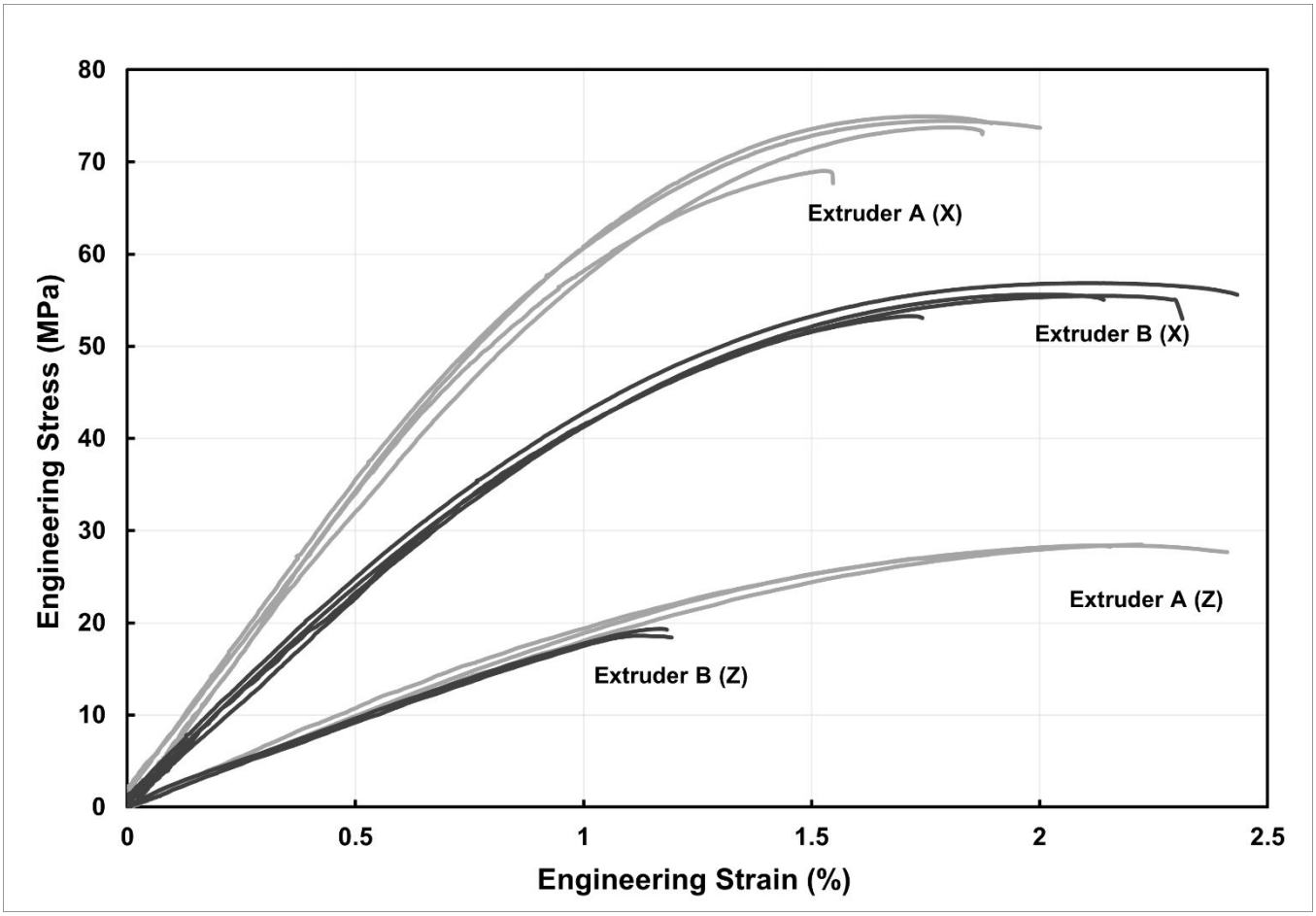

Figure 12: Comparison of the measured mechanical performance of samples, cut in the X and Z directions, from material printed at 130°C using Extruders A and B, tested internally. Figure by authors.

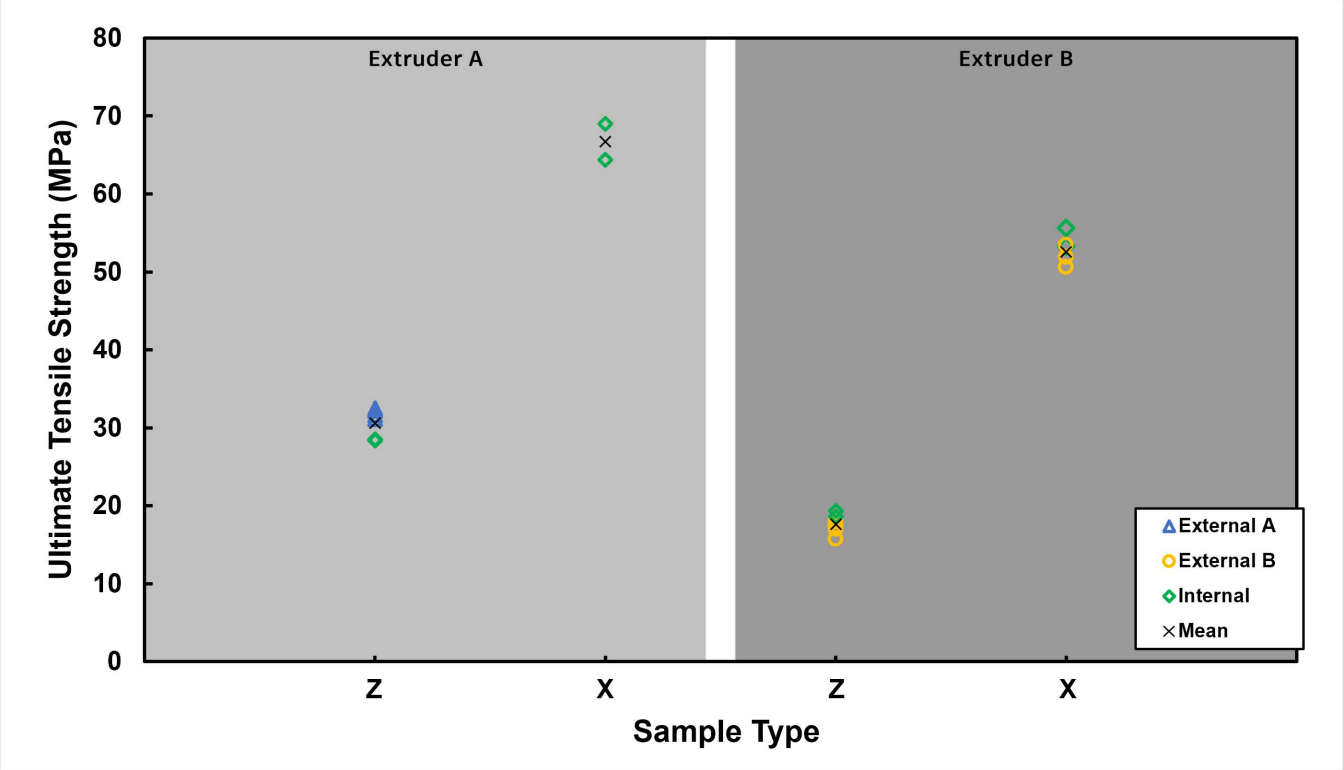

Figure 13: Comparison of Z and X tensile strengths for both extruders. Here it is shown that tensile strength in Z is measurably weaker than in X, regardless of the extruder used. Figure by authors.

Table 4: Comparison of Z and X tensile strengths for both extruders. Table by authors.

Sample Type	Mean UTS (MPa)	Standard Deviation	% of X Strength
Extruder A, Z direction	30.61	1.86	46%
Extruder A, X direction	66.70	3.27	
Extruder B, Z direction	17.60	1.17	33%
Extruder B, X direction	52.57	1.94	

For both extruders, the strength in the Z direction is measurably lower compared to the X direction: 46% and 33% depending on the extruder. This is in agreement with other studies that strength in the Z direction is significantly weaker, such as Somireddy et al. [7] who reported that Z (or "upright") samples of carbon fibre-reinforced ABS exhibited between 18-42% of the flexural strength of X (or "flat") samples.

Study 5: As-printed vs Planed surfaces

To assess the impact of surface finish on the measured mechanical performance of the material testing, some samples were planed to a smooth finish. Figure 14 and Figure 15 show a comparison between samples that were left as-printed and those that were planed to remove the 3D printed ridges. This figures exclusively shows results of tests conducted at Autodesk Materials Lab.

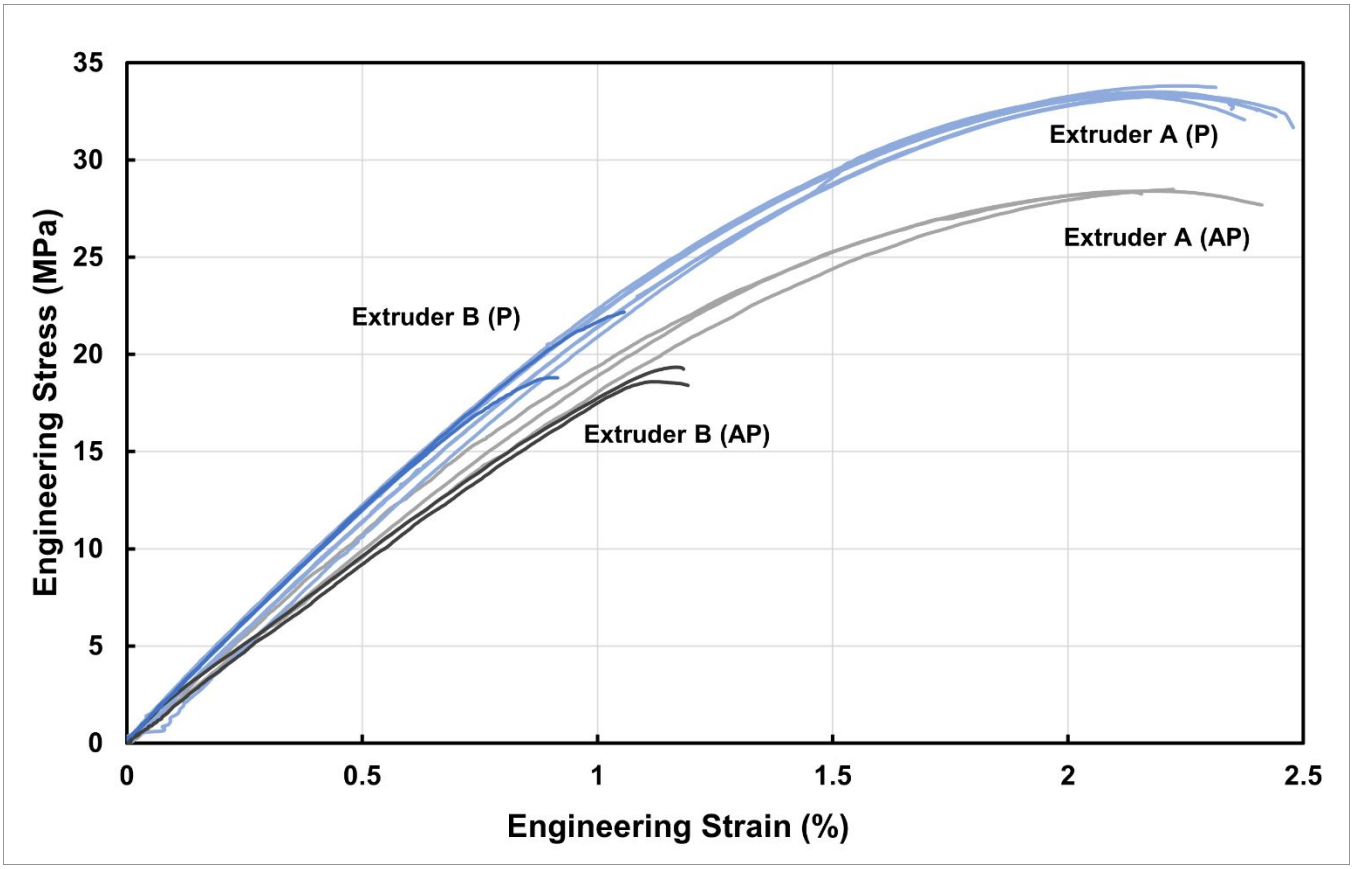

Figure 14: Comparative Engineering Stress-Strain curves for 'As-Printed' (AP) and Planed (P) Z Samples from both extruders. This figure illustrates the differences in tensile properties, contrasting the actual performance with the ideal mechanical properties of the manufactured material. Figure by authors.

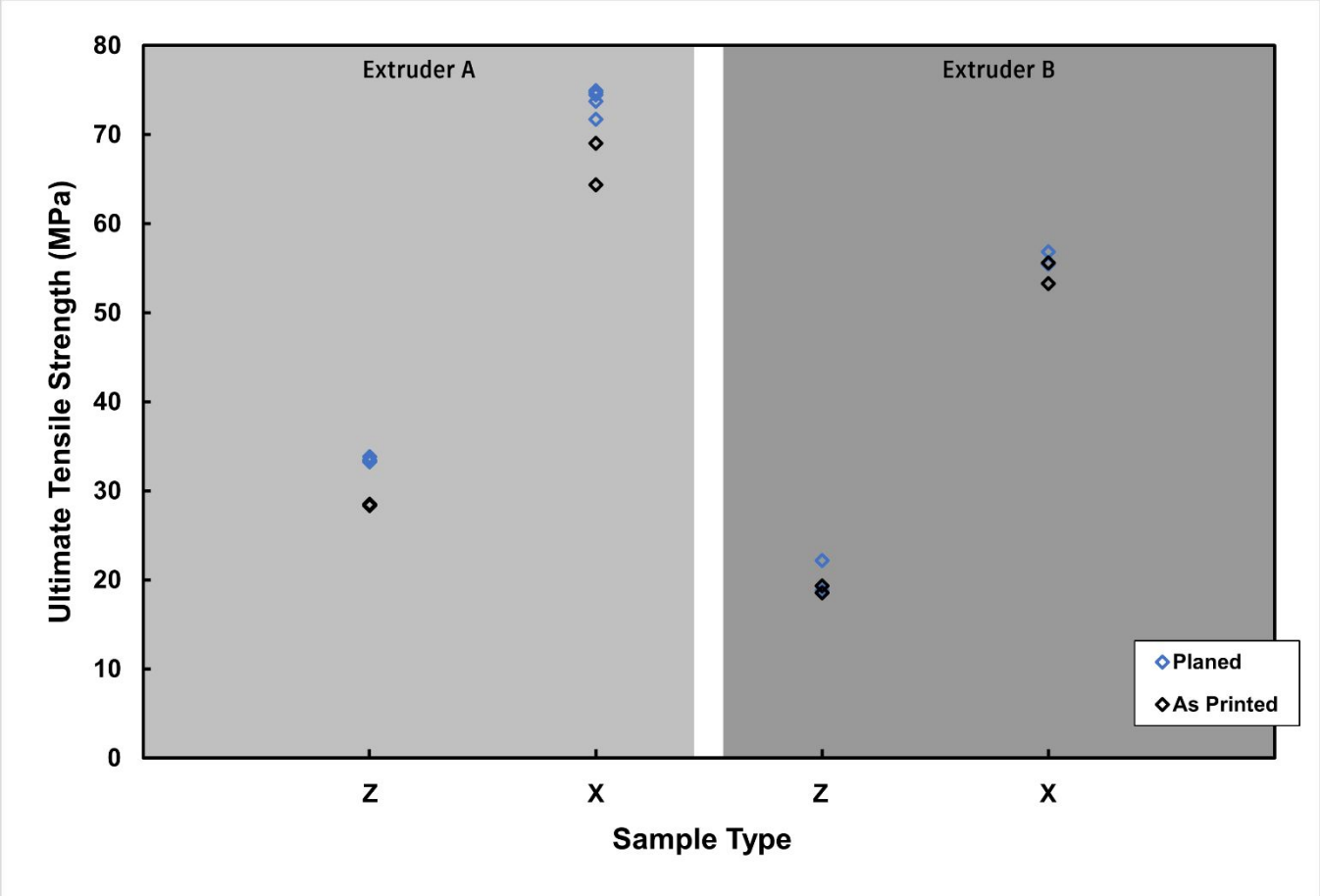

Figure 15: As-printed vs planed surfaces. Figure by authors.

Table 5 As-printed vs planed surfaces. Values are presented with their respective standard deviations (±). Table by authors.

	Sample Type	Sample Size	Mean UTS (MPa)	% Difference
Extruder A	Z, As Printed	3	28.4 ± 0.1	
	Z, Planed	6	33.4 ± 0.2	18%
	X, As Printed	2	66.7 ± 3.3	
	X, Planed	5	73.9 ± 1.3	11%
Extruder B	Z, As Printed	2	19.0 ± 0.5	
	Z, Planed	2	20.5 ± 2.4	8%
	X, As Printed	2	54.5 ± 1.6	
	X, Planed	2	56.2 ± 1.0	3%

These results suggest that planed samples exhibit higher tensile strength compared to their as-printed counterparts. It is important to acknowledge the limited sample size and the assumptions made about cross-sectional area, both of which warrant further discussion.

Study 6: Environmental temperature variation

Figure 16 shows the comparison of samples tested with an environmental chamber at -20°C and 70°C, and samples tested in ambient conditions without an environment chamber. All samples were planed. All samples were tested at Autodesk Materials Lab.

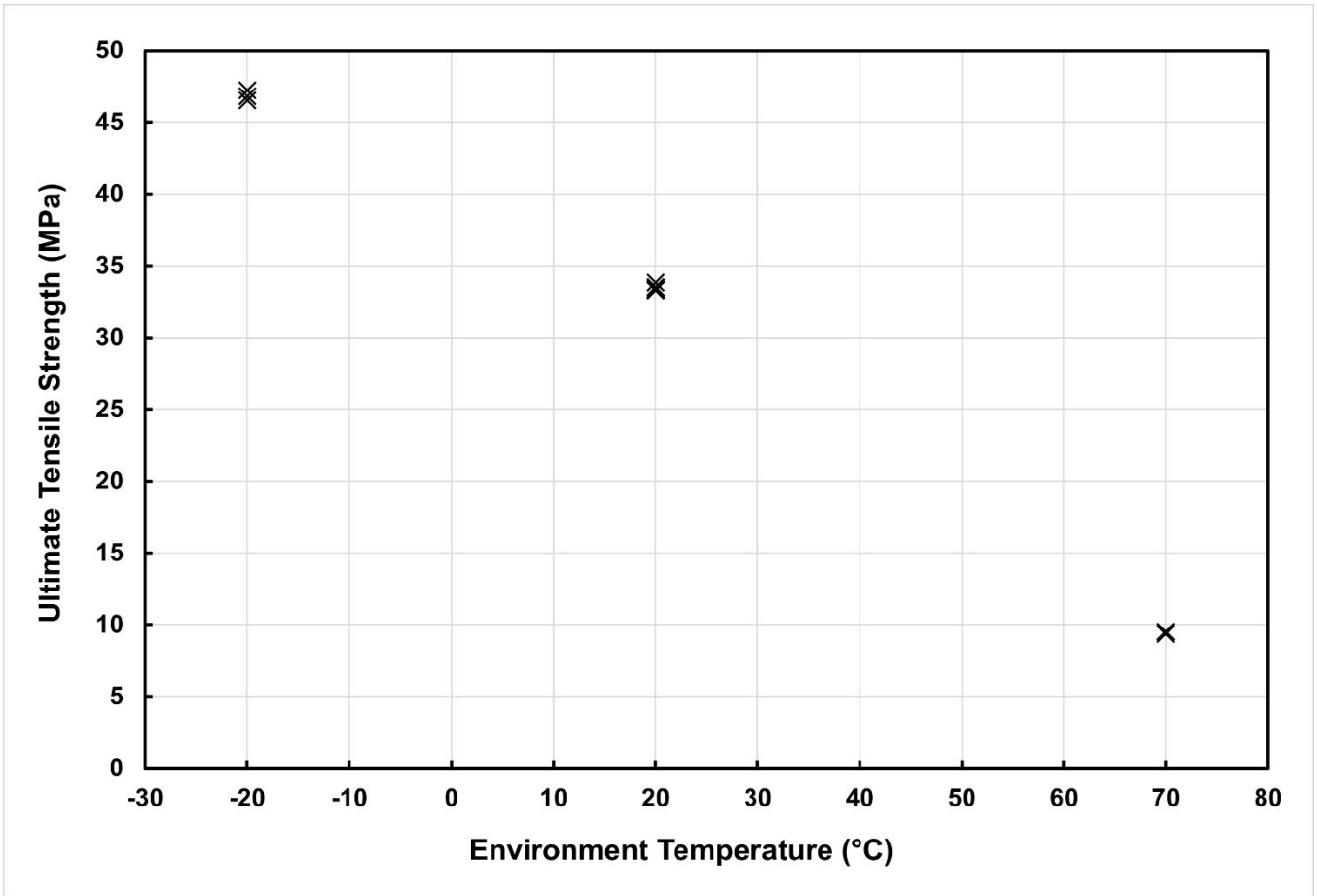

Figure 16: Comparison of tests conducted at different environmental temperatures. All samples from Extruder A, printed at 130°C, planed, and tested at Autodesk Materials Lab. Figure by authors.

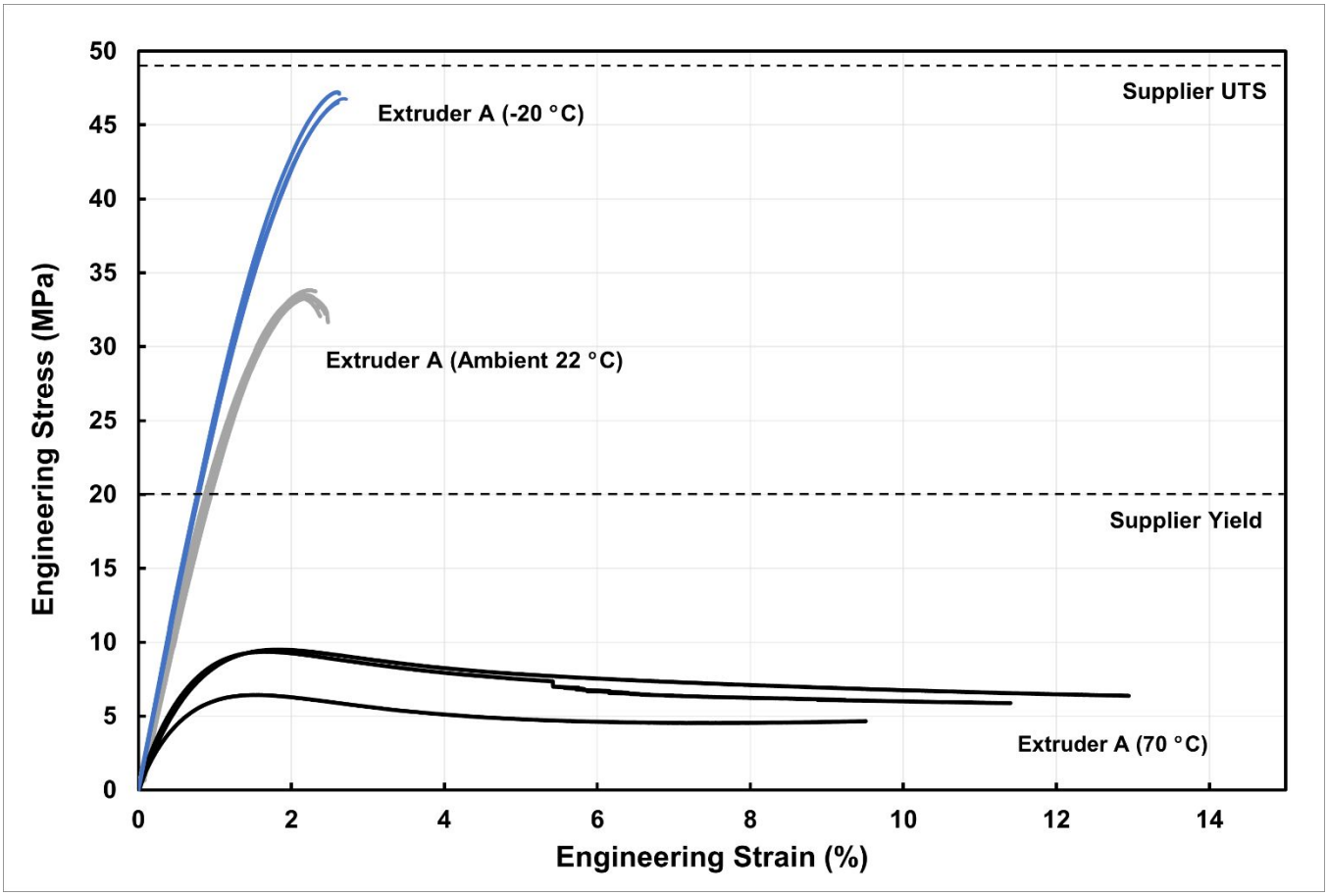

Figure 17: Stress-Strain curves illustrating the impact of varying temperatures on the measured mechanical strength of material tested exclusively with Extruder A. Figure by authors.

The results in Figure 16 and Figure 17 clearly illustrate the temperature dependency of strength for this material. There is a 28% decrease in measured UTS between -20°C and 20°C. There is an additional 70% decrease in measured UTS between 20°C and 70°C. Interpolating this data would suggest that at a peak habitable temperature of 45°C, the measured strength would be circa 20 MPa. Values for the Yield Strength and UTS as reported by the supplier are included for reference [23].

Study 7: Compressive Strength

Table 6 presents the results from compressive strength studies. All compressive strength tests were conducted with specimens from Extruder B at Autodesk Materials Lab.

Table 6 Compressive Strength study results. Values are presented with their respective standard deviations (±). Table by authors.

Sample Type	Sample Size	Mean Compressive Modulus (GPa)	Mean Ultimate Compressive Stress (MPa)	Mean Compressive Stress at Yield (MPa)
X	5	4.6 ± 0.5	70.4 ± 1.4	52.9 ± 4.8
Z	5	2.6 ± 0.2	50.5 ± 1.3	28.7 ± 5.6

Study 8: Shear Strength

Table 7 presents the results of the Shear Strength study. All tests were conducted with specimens from Extruder B at testing facility External B.

Table 7 Shear Strength study results. Values are presented with their respective standard deviations (±).

Sample Type	Sample Size	Mean Shear Modulus (GPa)	Mean Ultimate Shear Stress (MPa)
X	5	0.84 ± 0.04	25.18 ± 0.54
Z	5	0.74 ± 0.04	22.27 ± 0.72

These results suggest the polymer exhibits robust resistance to shear stress, with a mean value between 22 and 25MPa depending on the direction of applied load. This underscores the material's suitability for applications demanding durability and load-bearing capabilities. The ‘Z’ samples were weaker than the ‘X’ samples on average, which is as expected given the shear force is applied between layers. The reduction in shear strength in the ‘Z’ samples is 11.5%.

DISCUSSION

The relationship between Glass Transition Temperature and Interlayer Strength

The results of DSC suggested a T_g for this material of 72±0.5°C. This is lower than the range quoted in literature for virgin PETG [12,14,15,16]. The lower T_g is likely influenced by additional heat cycles experienced during recycling and printing, as well as by the material's glass fibre content. As will be discussed below (under Determining Optimal Printing Parameters), this value for T_g is lower than is required for a sufficient interlayer bond. Therefore, in opposition to the original hypothesis, it is not suggested that this is an adequate measure for the minimum interlayer temperature for this or other FGF materials. Instead, it is recommended that similar interlayer temperature studies are conducted as are presented in Study 2. With data collected across a wider range of materials, it may be possible to define a relationship that uses T_g to predict optimal printing temperatures.

Determining Optimal Printing Parameters

The results presented in Study 2 and illustrated in Figure 9 show an upward trend in the mean measured UTS, peaking at 130°C. This agrees with the previously proposed hypothesis: at lower interlayer temperatures, the mean UTS value in the Z-direction is lower. However, a more nuanced assessment is that there is a peak UTS at circa 30 MPa for most sample groups, but a high degree of variability in the measured UTS at lower T_p values, which suggests that premature failure is occurring more frequently and more severely as interlayer temperature decreases, rather than representing a clear and precise reduction in UTS as might be concluded by reading the mean UTS values in isolation. The high variability of measured UTS in the lower T_p samples presents a challenge in determining a representative UTS for these temperature ranges, and as such, it is suggested that these temperatures do not fall within the optimal processing window, and parts manufactured at these temperatures are at a higher risk of premature failure.

It is statistically significant that all sample sets, except for the 130°C set, have a maximum UTS of circa 30MPa, whereas the 130°C sample set has no values lower than this value. A larger sample set is necessary to draw stronger conclusions on optimal temperature, especially with 20°C intervals between sample sets. For the sake of the project for which these studies were conducted, it is reasonable to conclude that the optimal previous layer temperature T_p for printing with this material is 130±10°C.

Maintaining a T_p of 130±10°C for an entire print project would be very difficult to achieve, so a satisfactory margin for error was discussed. The results from tests at 150°C are very consistent, and therefore offer high certainty that material properties will be as expected, but on a larger and more complex print, there is a significant risk of material sagging if interlayer temperature exceeds 150°C in any areas. As such, an upper limit of 150°C was set, with intent to stay comfortably below this temperature.

A lower limit is more subjective, based on the strictness of the part requirements. As shown in Figure 18, if any strength greater than 80% of the maximum UTS is acceptable, the minimum UTS will be 26 MPa, and the minimum allowable previous layer temperature, annotated below as the critical temperature T_c, is in the region of 113°C.

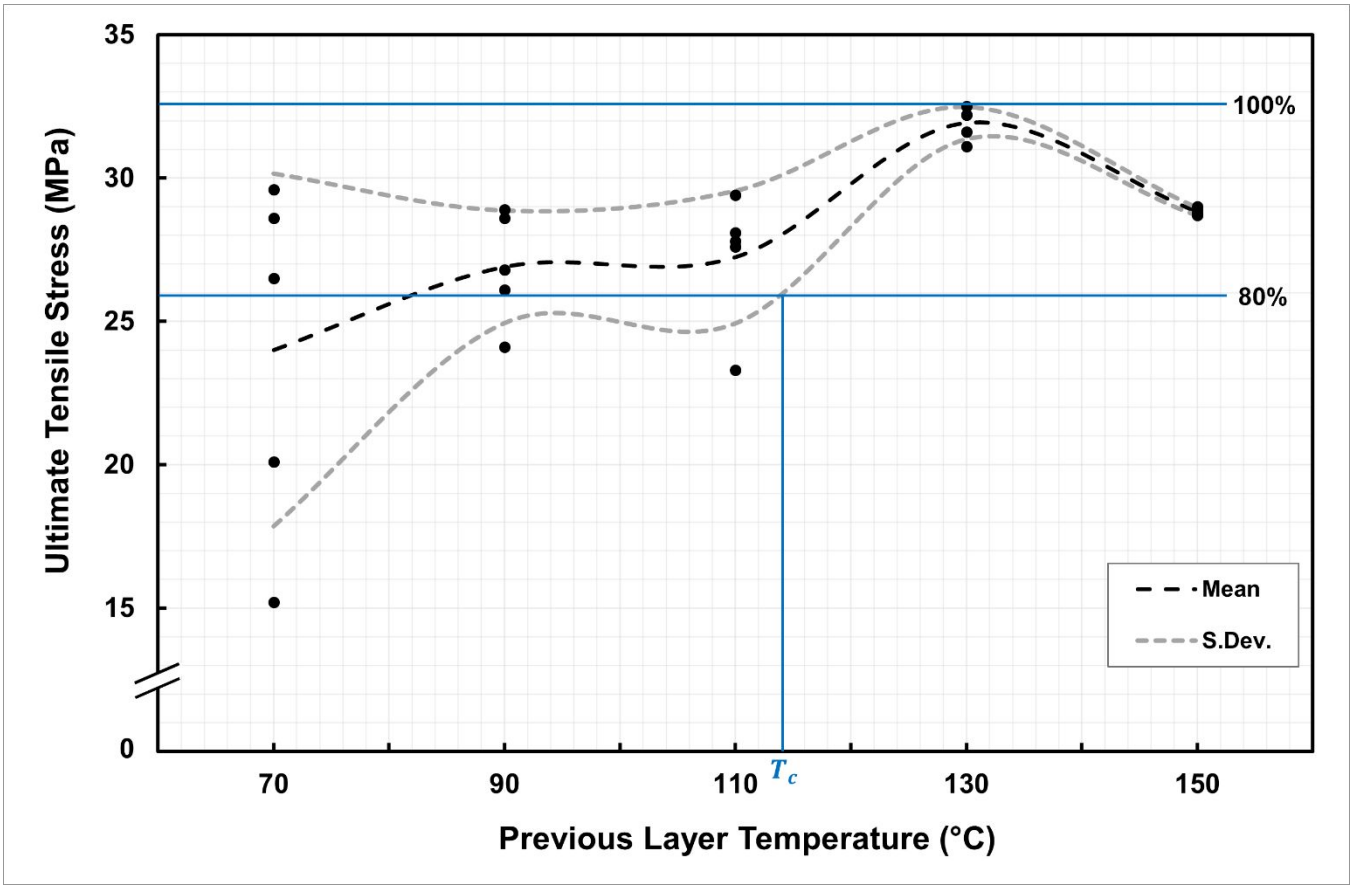

Figure 18: Ultimate Tensile Stress (UTS) plotted against Previous Layer Temperature T_p, with the critical temperature T_c indicated as the minimum temperature required to ensure 80% of the maximum part strength, based upon the results of this study. Figure by authors.

However, when marking the lowest value from the 110°C sample set as an outlier, the relationship is greatly strengthened, meaning that the previous layer temperature T_p can be much lower before the Standard Deviation curve drops below 26MPa. As such, it was further deemed acceptable to consider the minimum allowable temperature to be aligned with this newly presented lower-bound of standard deviation, meaning that the minimum previous layer temperature to achieve 26MPa would be approximately 93°C.

Given that Z strength is effectively reliant on the "weakest link in the chain", outliers like the one identified above will still likely play a role in any failure mode. It was hence acknowledged that the aim should be to maintain a part temperature higher than this minimum temperature where reasonably practicable. As such, Figure 19 illustrates the methodology taken when printing the final bridge.

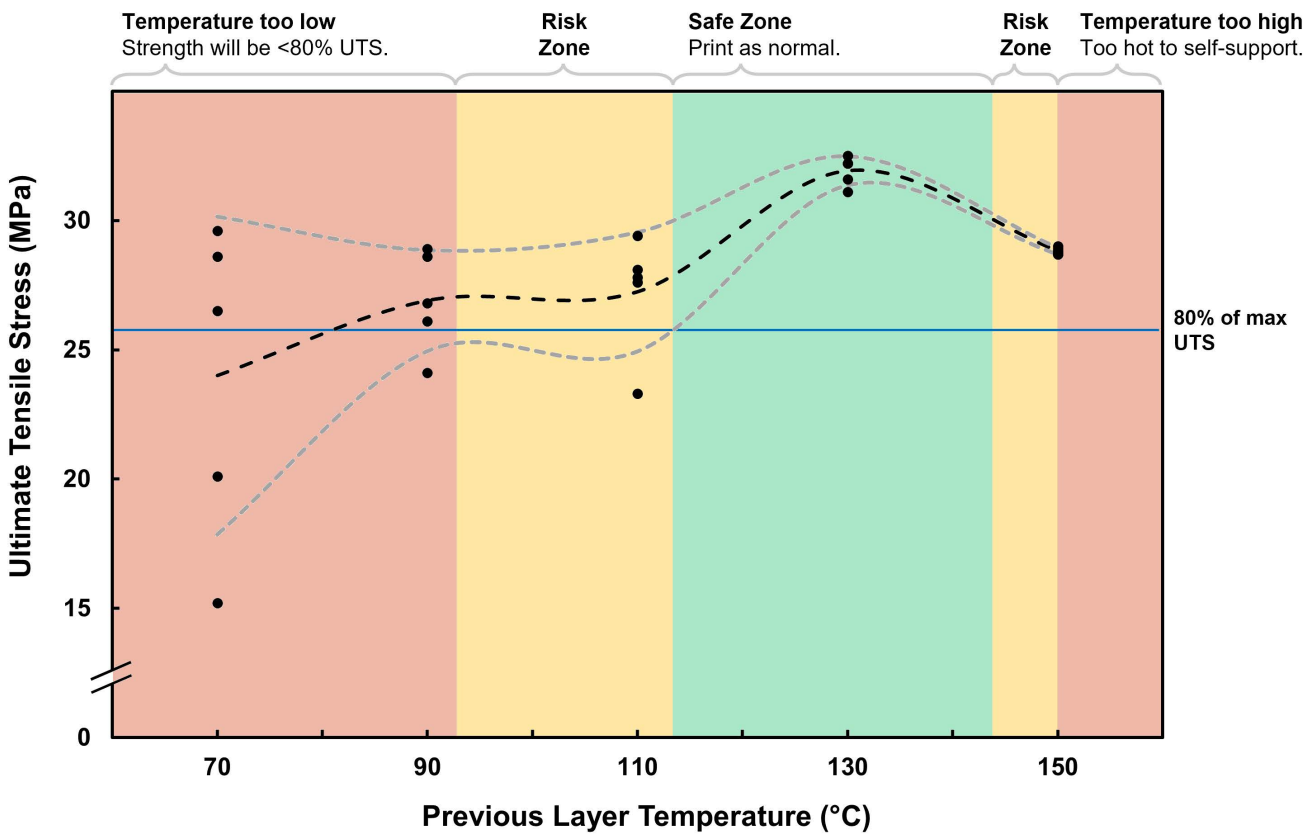

Figure 19: An annotated version of Figure 18, displaying temperature regions that could be considered during a real print project. The left-hand risk zone illustrates the region between 93°C and 113°C, with reasoning explained above. The right-hand risk zone represents a safety margin to the temperature where the material will no longer be self-supporting. Figure by authors.

Any recorded temperatures that fall in the red regions would be unacceptable. Any temperatures within the amber regions should be recorded and closely monitored to ensure these temperatures are not consistently repeated on consecutive layers. Any temperatures in the green region could be considered as safe.

Effective Cross-section Area

The dog-bone specimens were tested as-printed in most of the studies, meaning that the characteristic ridged surfaces were not milled flat. This ensured maximum relevance to the application, which also did not receive a milled finish, while introducing an area for significant discussion. The cross-section of the dog-bone specimens is illustrated in Figure 20. The red regions illustrate the assumed geometry of the specimens used in calculations based on the measured thickness. In reality, the effective cross-section area (CSA) may be more accurately taken as the grey cross-sectional region, which illustrates the true geometry produced.

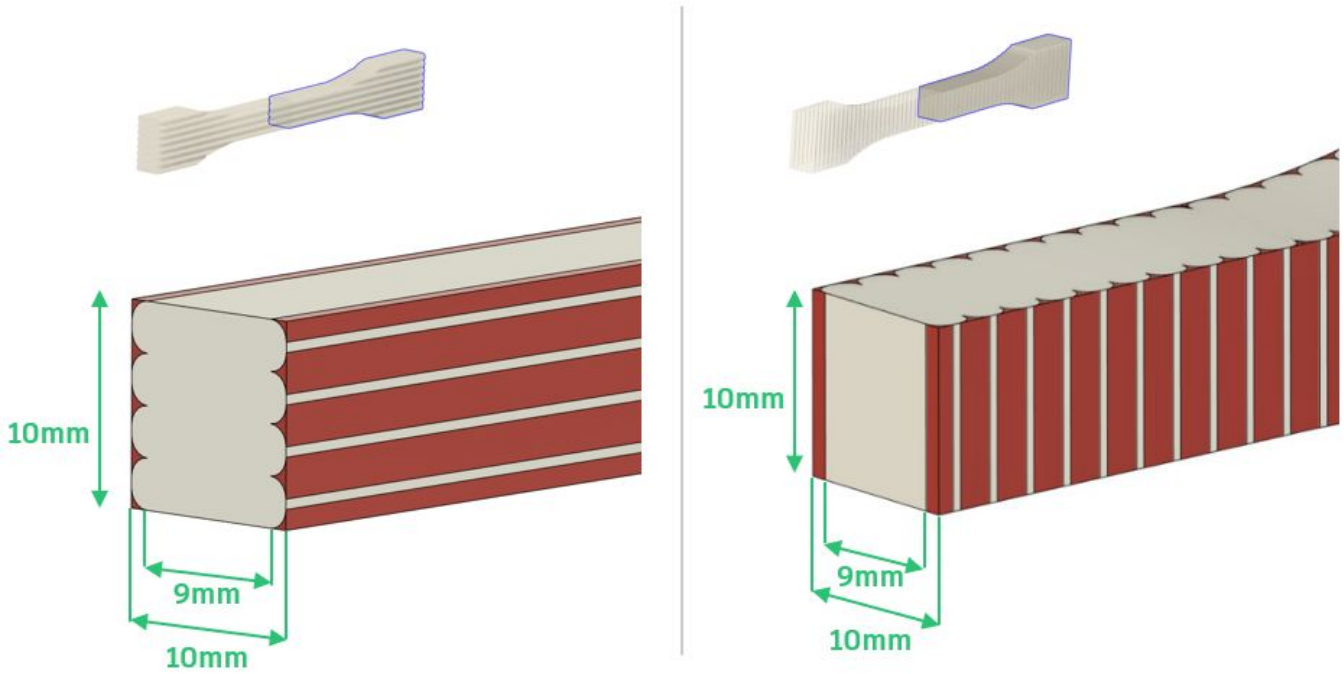

Figure 20: Illustration of cross-sectional profile of the dog-bone specimens. Left: Horizontal (X) specimen. Right: Vertical (Z) specimen. Figure by authors.

This is supported by the results of Study 5: As-printed vs Planed surfaces, presented in Table 5. The mean UTS for all planed specimen sets was higher, which implies that accounting for the effective CSA for the as-printed sets will give more consistent values when compared to the planed results.

Table 8 is a modified version of Table 5, showing the as-printed values with a correction for the effective CSA of Extruder A samples, assuming a cusp size of 0.5mm.

Table 8: A modified version of Table 5, showing the corrected UTS with a more representative effective CSA for as-printed samples. The correction illustrates an improvement in consistency after correction. Table by authors.

Sample Type	Sample Size	Mean UTS (MPa)		% Difference in UTS	
		As Tested	Corrected for Cusps	As Tested	Corrected
Z, As Printed	3	28.4±0.1	31.5		
Z, Planed	6	33.4±0.2	-	18%	6.3%
X, As Printed	2	66.7±3.3	73.6		
X, Planed	5	74.0±1.3	-	11%	0.5%

Extrapolating these results for larger and more complex models will introduce further levels of uncertainty. It is common for parts to be printed with a double perimeter wall, meaning the effective CSA will be proportionally larger than for a single-walled specimen such as those tested in the studies above. The most suitable approach would be to oversize the print such that the effective CSA meets the boundaries of the designed part. Any dimensionally critical areas can and should be machined to realise the net shape of the intended design, but the majority of the part will be oversized. This concept is illustrated in Figure 21.

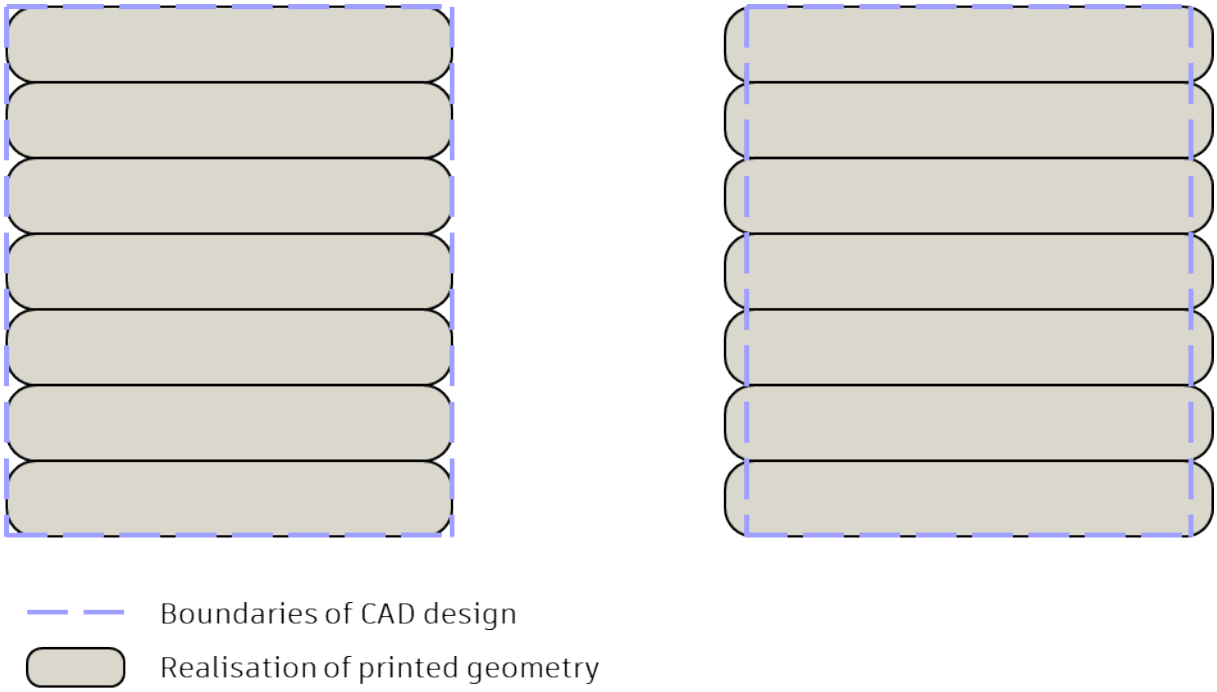

Figure 21: Two printing methodologies. Left: Print path remains entirely within the designed CAD boundaries. Right: Print path extends beyond CAD boundaries to ensure the effective CSA covers the entire designed geometry. Figure by authors.

Limitations and future work

The approach taken to control the temperature will vary depending on the project being conducted; the learnings from this paper were directly applied in the fabrication of a 5m-long bridge, as presented in Storey et al. [8](forthcoming). There is further discussion in this paper on the use of IR lamps to slow the rate of cooling over the entire print, rather than locally and rapidly reheating. On occasions where layer time was too long to maintain a temperature above the critical temperature T_c, printing was paused and IR lamps were stationed close to the printed part for a longer period of time until the surface of the part reached a stable temperature sufficiently higher than T_c.

Other material characterisation is needed for a full understanding of the performance of these materials in civil engineering settings over many years, including the effect of UV, moisture aging, and flammability. These were not tested in the scope of this project.

CONCLUSION

This study has made strides in understanding the relationship between the previous layer temperature (T_p) and the ultimate tensile strength (UTS) of parts fabricated using Fused Granulate Fabrication of MCPP's post-industrial PETG (PIPG). The investigation revealed an optimal T_p range of 130±10°C, where the interlayer bonding, and thus material properties, are at a maximum. At this temperature, the mean tensile strength in the vertical (Z) direction was calculated as 31.9MPa. However, maintaining this temperature for the duration of the printing process can be challenging; therefore, a practical margin for error was considered.

The high variability in UTS at lower T_p values suggests a higher risk of premature failure for parts fabricated at these temperatures. As such, the study identifies a critical temperature (T_c) around 113°C as the lower bound to achieve at least 80% of the maximum part strength, and an upper limit of 150°C to avoid material sagging. By taking into consideration the standard deviation and eliminating outliers, the minimum T_p to attain 80% of the maximum part strength was found to be approximately 93°C.

Additionally, the study highlighted the importance of considering the effective cross-sectional area (CSA) as opposed to the nominal CSA. The ridged surface characteristic of as-printed samples requires accounting for the effective CSA to obtain more consistent values. For larger and more complex models, the study recommends oversizing the print so that the effective CSA meets the designed part dimensions.

Results from differential scanning calorimetry (DSC) indicate a T_g of 72±0.5°C. This finding does not suggest a clear relationship between the glass transition temperature and the recommended interlayer temperature region presented in this paper. Further testing with a range of materials is recommended before such a relationship could be inferred.

Limitations of this study include unexplored factors such as the effects of ultraviolet radiation, aging, and flammability on the materials in civil engineering applications. These aspects warrant further investigation for a comprehensive understanding of material performance over extended periods.

The study suggests employing infrared heat lamps for slowing the rate of cooling over the entire print. This ensures that the material stays within the safe temperature range identified in this study. Future research could investigate alternative methods of temperature control that ensure sustained interlayer bonding and optimal material properties.

In conclusion, this study provides insights and recommendations for determining the optimal printing parameters in Fused Granulate Fabrication. Through analysis of the UTS and previous layer temperature relationship, this research contributes to enhancing the quality and reliability of printed parts. In turn, this has direct implications for the utilisation of additive manufacturing in civil engineering and other applications. Future research should consider the long-term effects and environmental factors on the material properties to further strengthen the application of this technology in real-world scenarios.

Acknowledgements
The authors would like to express their gratitude to our colleagues and friends at Dar Al-Handasah, particularly Ghassan Zein, George Marj, and Charles Malek, for their crucial commitment to, and advocacy for, this project. We also extend our thanks to our colleagues at Autodesk Research and the wider company, especially James Donnelly, Brandon Cramer, Stefanie Pender, Nic Carey, and Samer Bakdach. Our appreciation goes to the teams at the Autodesk Technology Center in Boston, Autodesk Technology Centre in Birmingham, and the Autodesk Materials Lab in Kilsyth for their indispensable facilities and support. Finally, we are grateful to Mitsubishi Chemical for their collaborative spirit and vital contributions to the success of this project.

Funding
This was an internal collaboration between Autodesk and Dar Al-Handasah. This research did not receive any specific grant from funding agencies in the public, commercial, or not-for-profit sectors.

Declaration of generative AI and AI-assisted technologies in the writing process
During the preparation of this work the authors used OpenAI's GPT-4 architecture to assist with readability and brevity in select areas. This tool was employed as a source of inspiration and to enhance clarity, with the final content being independently developed and rewritten by the authors. The authors take full responsibility for the content of the publication.

REFERENCES

[1] H. Al Jassmi, F. Al Najjar, A.-H. I. Mourad, Large-Scale 3D Printing: The Way Forward, IOP Conference Series: Materials Science and Engineering. 324 (2018) 012088. https://doi.org/10.1088/1757-899X/324/1/012088.
[2] A. Puzatova, P. Shakor, V. Laghi, M. Dmitrieva, Large-Scale 3D Printing for Construction Application by Means of Robotic Arm and Gantry 3D Printer: A Review, Buildings. 12(11) (2022) 2023. https://doi.org/10.3390/buildings12112023.
[3] A.L. Woern, D.J. Byard, R.B. Oakley, M.J. Fiedler, S.L. Snabes, J.M. Pearce, Fused Particle Fabrication 3-D Printing: Recycled Materials' Optimization and Mechanical Properties, Materials. 11 (2018) 1413. https://doi.org/10.3390/ma11081413.
[4] A. Roschli, K.T. Gaul, A.M. Boulger, B.K. Post, P.C. Chesser, L.J. Love, F. Blue, M. Borish, Designing for Big Area Additive Manufacturing, Additive Manufacturing. 25 (2019) 275-285. https://doi.org/10.1016/j.addma.2018.11.006.
[5] J. Kalle, K. Joni, S. Alexander, Potential and Challenges of Fused Granular Fabrication in Patternmaking, Inter Metalcast. (2023). https://doi.org/10.1007/s40962-023-00989-9.
[6] V. Kishore, A. Nycz, J. Lindahl, C. Duty, C. Carnal, V. Kunc, Effect of infrared preheating on the mechanical properties of large format 3D printed parts, In 2019 International Solid Freeform Fabrication Symposium. http://dx.doi.org/10.26153/tsw/17382.
[7] M. Somireddy, A. Czekanski, Anisotropic material behavior of 3D printed composite structures – Material extrusion additive manufacturing, Materials & Design. 195 (2020) 108953. https://doi.org/10.1016/j.matdes.2020.108953.
[8] P. Storey, N. King, J. Donnelly, S. Al-Ariss, Design for Additive Construction: Uncovering Challenges and Opportunities through the Robotic 3D Printing of a Pedestrian Bridge. (Forthcoming).
[9] I.M. Kalogeras, H.E. Hagg Lobland, The nature of the glassy state: Structure and glass transitions, Journal of Materials Education. 34(3-4) (2012) 69-94.
[10] P. Chesser, B. Post, A. Roschli, C. Carnal, R. Lind, M. Borish, L. Love, Extrusion control for high quality printing on Big Area Additive Manufacturing (BAAM) systems, Additive Manufacturing. 28 (2019) 445–455. https://doi.org/10.1016/j.addma.2019.05.020.
[11] V. Kishore, C. Ajinjeru, A. Nycz, B. Post, J. Lindahl, V. Kunc, C. Duty, Infrared preheating to improve interlayer strength of big area additive manufacturing (BAAM) components, Additive Manufacturing. 14 (2017) 7–12. https://doi.org/10.1016/j.addma.2016.11.008.

[12] Latko-Durałek, P., Dydek, K. & Boczkowska, A. Thermal, Rheological and Mechanical Properties of PETG/rPETG Blends. J Polym Environ 27, 2600–2606 (2019). https://doi.org/10.1007/s10924-019-01544-6
[13] N. Vidakis, M. Petousis, L. Tzounis, S.A. Grammatikos, E. Porfyrakis, A. Maniadi, N. Mountakis, Sustainable Additive Manufacturing: Mechanical Response of Polyethylene Terephthalate Glycol Over Multiple Recycling Processes, Materials. 14 (2021) 1162. https://doi.org/10.3390/ma14051162.
[14] S.-D. Sava, N.-M. Lohan, B. Pricop, M. Popa, N. Cimpoeșu, R.-I. Comăneci, L.-G. Bujoreanu, On the Thermomechanical Behavior of 3D-Printed Specimens of Shape Memory R-PETG, Polymers. 15(10) (2023) 2378. https://doi.org/10.3390/polym15102378.
[15] R.B. Dupaix, M.C. Boyce, Finite Strain Behavior of Poly(Ethylene Terephthalate) (PET) and Poly(Ethylene Terephthalate)-Glycol (PETG), Polymer. 46(13) (2005) 4827-4838. https://doi.org/10.1016/j.polymer.2005.03.083.
[16] S. Guessasma, S. Belhabib, H. Nouri, Printability and Tensile Performance of 3D Printed Polyethylene Terephthalate Glycol Using Fused Deposition Modelling, Polymers (Basel). 11(7) (2019) 1220. https://doi.org/10.3390/polym11071220.
[17] T. Wang, P. Consul, D. Bublitz, K. Drechsler, Continuous Directed Laser Preheating of Big Area Additive Manufacturing, Proposed for publication the Twenty-Third International Conference on Composite Materials (ICCM23), (2023).
[18] METTLER TOLEDO, Thermal Analysis of Polymers. Part 1: DSC of Thermoplastics, in Thermal Analysis UserCom 31, Application No. UC 311, (2011). https://www.mt.com/dam/non-indexed/po/ana/ta-applications/UserCom311.pdf. Accessed 4 September 2023.
[19] ISO (International Organization for Standardization), Plastics — Determination of Tensile Properties — Part 2: Test Conditions for Moulding and Extrusion Plastics, (ISO 527-2:2012), (2012). https://www.iso.org/standard/56046.html. Accessed 4 September 2023.
[20] ASTM International, Standard Test Method for Compressive Properties of Rigid Plastics (ASTM D695-15), Book of Standards Volume: 08.01, (2015). https://www.astm.org/d0695-15.html. Accessed 4 September 2023.
[21] ASTM International, Standard Test Method for Shear Properties of Composite Materials by the V-Notched Beam Method (ASTM D5379/D5379M-19e1), Book of Standards Volume: 15.03, (2021). https://www.astm.org/d5379_d5379m-19e01.html. Accessed 4 September 2023.
[22] TA Instruments, Discovery DSC, (2019). https://www.tainstruments.com/wp-content/uploads/Discovery-DSC-Brochure.pdf. Accessed 4 September 2023.
[23] Mitsubishi Chemical, FGF Recycled PIPG. https://mitsubishi3d.com/products/fgf-recycled-pipg/. Accessed 7 November 2024.